



HHS Public Access

Author manuscript

J Photochem Photobiol A Chem. Author manuscript; available in PMC 2017 February 01.

Published in final edited form as:

J Photochem Photobiol A Chem. 2016 February 1; 316: 104–116. doi:10.1016/j.jphotochem.2015.05.033.

Fluorescence Phenomena in Nerve-Labeling Styryl-Type Dyes

Tiberiu M. Siclovan, Rong Zhang, Victoria Coterio, Anshika Bajaj, Dmitry V. Dylov, Siavash Yazdanfar, Randall Carter, Cristina A. Tan Hehir, and Arunkumar Natarajan*

GE Global Research, One Research Circle, Niskayuna NY 12309

Abstract

Several classes of diversely substituted styryl type dyes have been synthesized with the goal of extending their expected fluorescent properties as much towards red as possible given the constraint that they maintain drug-like properties and retain high affinity binding to their biological target. We report on the synthesis, optical properties of a series of styryl dyes (*d1-d14*), and the anomalous photophysical behavior of several of these Donor-Acceptor pairs separated by long conjugated π -systems (*d7-d10*). We further describe an unusual dual emission behavior with two distinct ground state conformers which could be individually excited to locally excited (LE) and twisted intramolecular charge transfer (TICT) excited state in push-pull dye systems (*d7, d9* and *d10*). Additionally, unexpected emission behavior in dye systems *d7* and *d8* wherein the amino- derivative *d7* displayed a dual emission in polar medium while the N,N-dimethyl derivative *d8* and other methylated derivatives *d12-d14* showed only LE emission but did not show any TICT emission. Based on photophysical and nerve binding studies, we down selected compounds that exhibited the most robust fluorescent staining of nerve tissue sections. These dyes (*d7, d9*, and *d10*) were subsequently selected for *in-vivo* fluorescence imaging studies in rodents using the small animal multispectral imaging instrument and the dual-mode laparoscopic instrument developed in-house.

Keywords

Styryl dyes; TICT emission; nerve labeling; dyes; laparoscopy; *in vivo* and *ex vivo* imaging; fluorescence imaging of nerves

Introduction

Nerves are often difficult to visualize during surgery, due to their intricacy and anatomical variations in their location.¹ As a result, unintended nerve injury has been recognized as an important cause of morbidity associated with several lifesaving surgical procedures such as

*Corresponding author. Tel.: 518-387-4772, natararu@ge.com.

Publisher's Disclaimer: This is a PDF file of an unedited manuscript that has been accepted for publication. As a service to our customers we are providing this early version of the manuscript. The manuscript will undergo copyediting, typesetting, and review of the resulting proof before it is published in its final citable form. Please note that during the production process errors may be discovered which could affect the content, and all legal disclaimers that apply to the journal pertain.

SUPPLEMENTAL MATERIAL

See Supplemental Material for detailed synthetic procedures for dyes *d1-d11* and the corresponding characterization of the compounds using NMR and other relevant spectroscopic analysis.

prostatectomy,^{2,3} thyroidectomy,^{4,5} rhytidectomy,⁶ and breast cancer surgery.⁷ The need for guidance during surgery has been recognized for about a decade, beginning with the evaluation of techniques employing pre-operative CT and MR imaging.⁸⁻¹¹ However, real time decision making has directed intraoperative identification efforts towards fluorescence imaging,¹² including approaches relying on visualizing the nerves based on contrast agents designed to elicit selective nerve fluorescence during surgery, reviewed recently.¹³

To facilitate clinical use, the ideal *in vivo* nerve contrast agent must be designed to cross the tight junctions of the blood nerve barrier, a crucial requirement for systemic injection. Thus, in addition to being fluorescent, the contrast agent should show high selectivity to a nerve target as well as exhibit properties of small molecules. The targeting moiety has to be inherently fluorescent because conjugating the targeting component to a fluorescent dye would significantly increase its molecular weight beyond the desirable range.

The styryl dye, BMB, (1,4-bis(*p*-aminostyryl)-2-methoxybenzene), developed to be a PET tracer for imaging myelin absorbs in the near-ultraviolet range and emits in the blue region.¹⁴ While it bound with high affinity to myelin extracts from brain, BMB suffered from poor aqueous solubility. Moreover, intraoperative imaging at wavelengths optimal for BMB produced high background in non-target tissue because tissue autofluorescence was high in this region. Using BMB as a starting point, we sought to explore whether chemical modifications applied to bis-styryl dyes^{15,16} would allow us to elaborate them into dyes having optical and biological properties suitable for their use in an intraoperative setting.

We have since reported on bis-styryl dyes (**d1**, **d7** and **d9**) for selectively targeting myelin basic protein (MBP), a major component of nerves,¹⁷⁻¹⁹ along with compact optical imaging instruments for open and minimal access surgeries.^{20,21} Following intravenous injection, these dyes visualized central and peripheral nerves *in vivo* with high contrast relative to the surrounding muscle tissue, despite absorbing and emitting in the visible region. The affinity for MBP was maintained provided certain structural features were conserved.²² We have shown that both the absorption and the emission maxima can be red-shifted significantly by employing through- π system conjugated donor-acceptor (D-A) group, producing dyes with large Stokes shifts, thus minimizing the impact of autofluorescence in the visible region.

Herein, we report the screening and optical characterization of a series of molecules (**d1-d14**) with the aim of creating dyes with red-shifted fluorescence, large Stokes shifts and high fluorescence yields while maintaining binding to nerves and improved aqueous solubility. Furthermore, we elaborate on the unusual photophysical properties of our previously reported fluorophores, which were observed for both *in-vitro* (in organic solvent) and *in-vivo* (in mouse nerves).

MATERIALS AND METHODS

Synthesis of dyes

The dyes shown in Table 1 were synthesized in step-wise procedures as illustrated in the Schemes below. Details of the synthetic methodology can be found in the Supplemental Material. Compounds were purified by medium performance liquid chromatography on

silica gel (ISCO Companion with RediSep Gold silica columns). Those selected for advancement into in vivo imaging studies were further purified by high performance liquid chromatography (HPLC). For normal phase HPLC, a Shimadzu LC-8A equipped with a SIL-10AP autosampler, an SPD-M20A diode array detector and an FRC-10 A fraction collector were used, together with a Waters Sunfire preparative silica OBD column, 5 μm , either 19 \times 150 mm or 50 \times 100 mm, and a hexanes/ ethyl acetate gradient. For reverse phase HPLC, a GE AKTA Avant system was used, with a Waters XTerra PrepMS C18 column, 5 μm , 30 \times 100 mm and water – 0.1% formic acid/ acetonitrile/ 0.1% formic acid gradient.

Bis-styryl dyes having three ring structures similar to that of **d7** (*vide infra*) have been synthesized following the methodology previously reported.¹⁸ Essentially, this consists of a tandem Heck coupling of the appropriately functionalized aminostyrene with the correspondingly substituted bromo arylaldehyde, followed by a Horner-Wittig olefination with the appropriately substituted benzyldiethyl phosphonate (Scheme 1).

Compounds **d5** and **d8** were prepared via reductive amination of **d1** and **d7**, respectively. Compound **d11** was prepared as illustrated in Scheme 2.

Compounds **d12** and **d14**, containing multiple electron withdrawing groups were prepared via a Knoevenagel condensation of the corresponding styryl aldehyde with the active methylene compounds, as described previously²³ and illustrated in Scheme 3 for compound **d14** and detailed in the experimental sections for compounds **d12-d14**.

The styryl compounds **d2-d4** have been prepared via straightforward transformations depicted in Scheme 4. Compound **d2** has been previously reported¹⁶ and has been included here for comparison within the polyene series. Updated reviews of the general methodologies described above have been published recently.²⁴⁻²⁶

Characterization of nerve labeling dyes

Methods for spectroscopic and physicochemical characterizations were as previously described.¹⁸ Briefly, absorbance spectra were taken using a Lambda 20 UV/Vis spectrometer (Perkin Elmer, Waltham, MA). The wavelength of maximum absorbance was then used as the excitation wavelength for the collection of the fluorescence emission spectra on a steady state fluorimeter (Photon Technology International, Birmingham, NJ). A 10 mM stock solution of each dye in dimethylsulfoxide (DMSO) was used in the preparation of 10 μM solutions of the dye in DMSO, unless indicated otherwise.

Ex vivo and in-vivo imaging

Ex vivo nerve tissue staining on each of the dye was performed as described.¹⁷ A buffer only control (no dye) was performed using exactly the same procedure to determine autofluorescence under identical imaging settings.

In vivo nerve imaging studies on selected dyes were described previously.^{18,27} All procedures were approved by the Institutional Animal Care and Use Committee at GE Global Research. Briefly, CD- 1 mice ranging in body weight from 25 to 30 g, and Sprague-Dawley rats ranging in body weight from 250 to 300 g, were purchased from Charles River

Laboratories (Wilmington, MA). On the day of the experiment, mice and rats were anesthetized using 2%–4% isoflurane and given a single tail vein injection each of 50 mg/kg of **d7** (GE3082), 8 mg/kg of **d9** (GE3111), or 12.2 mg/kg of **d10** (GE3126). The animals were then returned to the home cage until the designated time-point for imaging (3 h post-injection for **d7** and **d9**; 1 h post-injection for **d10**). The nerves were exposed and multispectral imaging was initially performed using a fluorescence stereomicroscope (SteREO Lumar V12, Carl Zeiss Inc., Thornwood, NY) equipped with a multispectral imaging camera (Nuance, CRI, Woburn, MA). Imaging using our custom laparoscopic instrument was as described.²⁷ Imaging of control animals (with no dye injected) was performed under identical conditions.

Spectral measurements of tissue fluorescence were done using a spectroscopic probe. The probe consisted of illumination (405 nm laser, which was the same as the laparoscopic instrument illumination, or a 447 nm laser) coupled to a fiber, a premium-grade reflection ferrule (Ocean Optics, 6 illumination fibers, 1 600-micron read fiber, 3-inch long ferrule), a collimator with a holder for excitation rejection filter, and a spectrometer (Ocean Optics, USB2000+UV-VIS). The 405 nm excitation spectra were measured with BLP01-405R-25 rejection filter, while the 447 nm excitation spectrum was measured with LP03-458RU long-pass filter.

RESULTS & DISCUSSION

We investigated the absorption and emission properties of dyes **d1-d14** in non-polar (toluene) and polar (DMSO, MeOH) solvents. The dyes **d1-d14**, shown in Table 1, can be classified into two categories, where dyes **d1-d5** have conjugated amine based electron donating “push-push” end groups, while **d6-d14** are based on electron-donating and electron-withdrawing “push-pull” end groups in conjugation. The purpose of screening these individual categories was to see which one of these gave the longest wavelength emission and highest fluorescence yields while maintaining nerve binding.

Since we had previously shown that BMB (**d1**) can bind and visualize nerves in vivo,¹⁹ we utilized this molecule as a starting point to develop dyes with improved optical properties. The absorbance and fluorescence emission maxima in DMSO for each synthesized dye are shown in Table 1. Compounds **d2** and **d3** lacking a central arene group (Scheme 4) displayed a hypsochromic shift in the absorption and emission while retaining high emission intensity as compared to **d1**. Compound **d4**, in which the central arene was preserved while incorporating an extra alkene on each side of the arene, showed a reasonable bathochromic shift of the emission compared to **d1**, however its fluorescence intensity was reduced dramatically (fluorescence emission intensity: **d1**=106,800 vs. **d4**=200). Alkylation of the amine groups (**d5**) helped in further bathochromic shift of absorption and emission with respect to **d1** while maintaining sufficient fluorescent intensity.

In the push-pull dye system category, **d6** was used as a model compound which displayed solvent dependent behavior; In the push-pull dye systems category, **d6** was used as a model compound which displayed solvent dependent behavior; absorption and emission maxima of 368 nm and 432 nm respectively in non-polar solvents (toluene). In polar solvent (DMSO),

d6 displayed an absorption maximum at 385 nm and emission maximum at 522 nm which we assign to a Twisted Intramolecular Charge Transfer (TICT) state.²⁸ Extending the conjugation of this system by adding an arene middle ring (**d7**) resulted in a bathochromic shift of ~30 nm in absorption and a dual emission in DMSO at 491 nm and 621 nm. The solvent dependent behavior of **d7** relative to the analogous non push-pull system (**d1**) is shown in Figure 1.

N-methylated dye system **d8** resulted in a slight (5 nm) hypsochromic shift of the absorption with a maximum at 412 nm and a modest 27 nm shift in emission, with respect to the short wavelength emission of the unalkylated amine dye system **d7**. To our surprise this system failed to show dual emission in polar solvents. Replacing the electron withdrawing cyano group with other electron withdrawing groups –SO₂Me, –SO₂-piperazine (**d9** and **d10**) showed similar absorption trends and values and large Stokes shifts, with emission maxima around 620 nm. Replacing the electron donating system –NH₂ by a hydroxy (–OH) group in **d11** resulted in a hypsochromic shift in absorption and emission with respect to **d6**. Similar to compounds **d7**, **d9** and **d10** also showed dual a emission in polar solvents.. Using the indoline or N,N-dimethyl amino groups as electron donating groups with a variety of electron withdrawing moieties such as dicyanovinyl, methylsulfonyl, dicyanopyranyl (**d12-d14**), resulted in bathochromic shifts in absorption (467, 419, and 482nm, respectively), and reasonable Stokes shifts albeit low emission yields.

To identify the most promising nerve labeling dyes, a qualitative ex vivo tissue staining assay was performed using each of the dye with detectable fluorescence. Figure 2 shows examples of microscopic images of fluorescently labeled rat nerve tissue sections. Here, compounds **d7**, **d9**, and **d10** exhibited the most robust fluorescent staining of nerve tissue sections. These dyes were subsequently selected for in vivo fluorescence imaging studies in rodents- using (1) the small animal multispectral imaging instrument shown in Figure 3; and (2) the dual-mode laparoscopic instrument developed in-house shown in Figure 4.²⁸

Figure 3 shows examples of multispectral imaging in mice. In general, the nerves appeared red-orange and the surrounding muscle tissue was dark. Because the dyes are lipophilic, there was some non-specific partitioning to adipose tissue which appeared as yellow-green fluorescence under the multispectral camera.

Figure 4 shows the dual-mode laparoscopic imaging of a rat injected with **d7**. Note the thin layer of fascia obscuring the nerve under white light imaging, but not under fluorescence visualization. More detailed in vivo dosing and kinetics results for these three dyes were described elsewhere (**d7**^{17,19,28}; **d9**¹⁸; manuscript submitted for **d10**);).

We have also developed a spectroscopic probe for exact spectral measurements of tissue fluorescence *in-situ*. The probe allows precise local measurement to be taken at a tissue of interest at a high-resolution (1 nm) and relatively small integration times, typically 1-2 sec for nerve, 0.5 sec for adipose tissue, and 2-5 sec for muscle. This spectral probe used the same illumination as the dual-mode laparoscopic instrument (405 nm excitation). Figure 5 shows spectral measurements of the nerve, adipose tissue, and muscle in a dissected mouse treated with of **d10**. The probe was pointed at the relevant tissue inside the mouse. The

shape and intensity of the spectrum for nerve, adipose tissue, and muscle was different from one another. The emission spectrum of the nerve was reminiscent of the dual emission wavelength observed in DMSO (Table 1),

Our approach to improving the photophysical properties from our initial model system BMB (**d1**) focused on increasing conjugation of the push-push based dye system, and investigating the effect of a series of push-pull based Donor-Acceptor (D-A) groups, conjugated across a variable length π -system, followed by down-selection and biological screening. Of particular interest was the number of connecting double bonds, the number of aromatic rings, and the strength of the acceptor group, including the effect of multiple acceptor groups. Additionally, we were presented with the challenge of having to determine what molecular characteristics were necessary to retain in order to maintain the binding affinity to our target of interest - myelin basic protein.¹⁷ In order to obtain reasonable solubility in the three ring system and attenuate lipophilicity we incorporated a methoxy- group in the middle aryl ring.²⁹

We sought to understand the influence of conjugation length in this structural space by extending the π -system *via* the addition of double bonds, an aim most readily achieved, from a synthetic point of view, in symmetrical D- π -D systems. Extending the conjugation of the simple 2-ring diaminostilbene **d2** by one double bond provided the expected, modest bathochromic (red) shift to both absorption and fluorescence emission. The same transformation applied to the 3-ring BMB system (compound **d1**) led to compound **d4**, in which the absorbance displayed a slight hypsochromic (blue) shift and the fluorescence was essentially suppressed. In agreement with previous reports on diene chromophores^{30,31} we are compelled to conclude that extended alkene systems such as **d4**, despite the addition of only one double bond on each side of a rigidifying middle ring, possess too flexible a backbone. Thus the fluorescence quantum yields and lifetimes in these systems are dependent on mechanisms that compete with non-radiative decay which do not lead to photoisomerization and might not involve large amplitude torsional motions. Through NMR and LC-MS analysis we established that isomerization to *cis*-products does not occur upon irradiation of our lead candidate dyes, **d7**, **d9** and **d10**. Similarly, in the *trans*-diphenylbutadiene system, Saltiel *et. al.*³⁰ have observed radiationless decay pathways that do not lead to photoisomerization resulting in the reduction of fluorescence quantum yields and lifetimes in contrast to the corresponding *trans*-stilbene derivatives.

Electronic Donor-Acceptor (push-pull) D- π -A systems, where D = $-\text{NH}_2$, $-\text{N}(\text{CH}_3)_2$, $-\text{OH}$ and A = $-\text{CN}$, $-\text{NO}_2$ etc., have been studied extensively for their tendency to exhibit large Stokes shifts and a solvent dependent dual fluorescence behavior.³² These observations have been explained using a three-state model as opposed to a conventional two-state model as seen in Figure 6, adapted from the work reported by Lapouyade and coworkers^{33,34} wherein LE* represents a highly polar, locally excited fluorescent state with planar geometry; A* represents a highly polar, TICT fluorescent state with a twisted group, and P* represents a weakly polar, non-fluorescent funnel to the ground state with twisting about the stilbene double bond. The dynamic transformation process between LE* and A* has been hypothesized to go through an energy barrier that has been shown to be sensitive to the polarity of solvents and the concentration of the dye.³³

We sought to exploit this effect in the bis-styryl system. Substitution of an electron-withdrawing cyano moiety for one of the amines in the two-ring stilbene (**d2**) led to a large Stokes shift as a result of accessing the ICT (A*) state.³⁵ Applying this same substitution to the three-ring BMB system (comparison of compounds **d7** vs. **d1**) led to a modest 9 nm bathochromic shift in the absorbance, a primary emission band at 491 nm attributed to the LE* state and an additional long wavelength emission attributed to the A* ICT state at 621 nm. Substitution with alternative electron withdrawing groups methylsulfonyl or sulfonamide, introduced to improve pharmacokinetics and pharmacology properties, (compounds **d9** and **d10**) resulted in similar shifts in absorption and emission. The long wavelength emission is only observed in polar solvents such as DMSO, Figure 7A, and providing further evidence in support of formation of an ICT state.

Alkylation of the amine in the 3-ring, D- π -D BMB system (**d1**) led to compound **d5** with a 7 nm bathochromic shift in absorption and a 16 nm shift in emission, as might be expected; however, the emission intensity was significantly reduced. Similar N-alkylation in the push-pull D- π -A system (**d8** & **d12**) led to complete suppression of the long wavelength emission. This observation is contrary to the behavior reported in the well-studied DMABN system in which aminobenzonitrile displayed emission only from the LE* state and N,N-dimethyl aminobenzonitrile displayed a long wavelength emission from the A* (ICT) state, in turn attributed to twisting about the aniline bond.³⁵ Gruen & Gerner also reported lack of dual emission in the 2-ring N,N-dimethylamino-4-cyanostilbene.³⁶ We hypothesize that the dissimilar emission behavior in the alkylated vs. non-alkylated 3-ring system may be due to a combination of twisting about the stilbene bonds and the presence of an electron-donating methoxy substituent in the central ring though more extensive photophysical studies are required to explain the behavior of this unique system

Further investigation of the four systems (**d7-d10**) uncovered an additional phenomenon which is unprecedented, at least in the case of the three-ring, push-pull stilbene systems. Compound **d7** showed a dual emission in a polar solvent (DMSO) similar to that of 4-amino-4'-cyanostilbene (ACS).³⁷ However, to our surprise, this dual emission displayed two distinct excitation bands at 380 and 420 nm respectively for the 491 nm (LE) and 621 nm (CT) emissions, yet only a single excitation and emission in a non-polar solvent (Figure 7). The wavelength dependent emission of compound **d7** is further illustrated by exciting from 300 nm-500 nm in 5 nm intervals and collecting the corresponding emission spectra in DMSO (Figure 8). The observed solvent dependence and large Stokes shift associated with the long-wavelength emission strongly support the assignment of dual emission peaks at 491 and 621 nm to LE and CT states respectively. The wavelength dependence and distinct excitation bands would suggest the excitation of two different species in polar media. We hypothesize that these may represent ground-state conformers that differ through twisting about one of the stilbene single-bonds and that one of these conformers has an arrangement that facilitates formation of the ICT state.

Recently, Atsbeha *et al.*³⁸ and Catalan *et al.*³⁹ reported that a similar trend was seen for DMABN in polar solvents. Catalan hypothesized that a dipolar solvent forms species with charge transfer properties in its ground electronic state and such forms can be directly excited to a TICT structure. However the anomalous behavior with the systems under our

study stems from the fact that while the amino derivative **d7** showed dual emission in a polar medium, the N,N-dimethyl derivative **d8** did not display the expected long-wavelength TICT emission. Compound **d8** showed a single LE emission maximum at 460 nm in non-polar medium (toluene) and a single emission peak maximum at 500 nm in polar medium (DMSO) as shown in Figure 7. Unlike DMABN where twisting of N,N-dialkyl group is responsible for TICT emission (Scheme 5), the push pull stilbene based system is known to undergo aniline moiety twisting which could also be thought to be responsible for dual emission characteristics.⁴⁰ Unlike 4-cyano-4'-amino stilbene systems in which twisting about the aniline bond represents the only degree of rotational freedom (Scheme 5), multiple ground state conformers that may exist in the three ring stilbene-type systems as shown in Scheme 6.

Thus, it was not surprising that compound **d7**, with a less bulky amino group, could still show a dual emission behavior in a polar solvent, as the dual emission in the stilbene type system does not depend on amine bond twisting. However, one would have expected the corresponding N,N-dimethyl system **d8** to still show at least a similar dual emission behavior, even if not a more pronounced effect. We believe that the *methoxy*-substitution has an important role to play for the dual emission behavior of **d7** and absence of the same in **d8**. Attempts to cross check if the *methoxy*-substituent is indeed responsible for the above emission behavior in **d7** and **d8** by making the parent tri-ring stilbene system without the *methoxy*-substituent was not pursued because this molecule was shown to be insoluble in polar solvents such as MeOH and DMSO.⁴¹ Recently Singh *et al.*⁴² reported a similar observation in the 1,2-diarylethene system having a linear acceptor group such as –CN on one of the phenyl rings and two electron donor groups such as –OMe on the other phenyl group, giving systems capable of solvent polarity-dependent dual fluorescence. The short wavelength fluorescence band was assigned to LE state, which is electronically delocalized with a planar geometry. The long wavelength fluorescence band has been attributed to a TICT state having a dipolar character. The authors reported that they couldn't determine the exact site of excited state bond twist leading to the formation of TICT species.

There is literature precedence for molecular structures that possess N,N-dimethyl substituted push-pull dyes which show no TICT emission. Since double bond rotation *trans*→*cis* is excluded in these systems, we hypothesized that the deactivation from the singlet-excited state is mainly achieved through an internal conversion mechanism in polar solvents. Fromherz, Heilmann and others reported that N,N-dimethyl substituted hemicyanine undergoes internal twisting and yields a twisted internal charge transfer (TICT) state on photoexcitation [Scheme 7].^{43,44} However, no dual emission was observed in this molecule (HC-3) and the authors hypothesized a non-emissive TICT state. Due to multiple bond rotations producing rotamers in hemicyanine dyes, the ICT states are deactivated. Strehmel and co-workers performed quantum mechanical calculations on various TICT conformations of hemicyanine dyes, and ruled out the possibility that deactivation of TICT state is due to twisting of diamino group, since this charge transfer state is approx. 1.5 eV higher in energy than that of the Frank–Condon state.⁴⁵ The authors attributed twisting of single bonds adjacent to the central double bond to the formation of CT states comparable in energy to that of the FC state and causing the singlet-excited state twisting of the aniline ring to

become barrierless in polar solvents. Fromherz also studied two other dye systems, (dimethylamino)methylazafluorenium with a rigid fluorene group [HC-3] and [(dimethylamino)phenyl]methylpyridinium [HC-2] with a freely rotatable biphenyl frame.⁴³ The quantum yield of the more rigid dye is around 50%, while the quantum yield of the twistable homolog is about 0.05% in solvents of high polarity and fluidity. The difference in the fluorescence behavior is attributed to the formation of a TICT state with efficient radiationless deactivation.

We investigated additional systems to verify that the emission behavior of compound **d7** and **d8** was neither a single anomaly nor an artifact. Compounds **d9** and **d10** are similar to Compound **d7** but the electron accepting –cyano group replaced by another electron accepting groups methylsulfonyl and piperazinylsulfonyl respectively. Compound **d9** and **d10** still showed similar LE and TICT dual emissions similar to that of **d7** and exhibited two ground state conformers that could be individually excited. Dual emission of compound **d9** in DMSO obtained using excitation wavelength 380 nm is shown in Figure 9.

A phenol replacing the amino group proved to be a much poorer donating group (compound **d11**) even under pH conditions which ensured complete deprotonation to the respective phenoxide resulting in hypsochromic shift by ~20 nm and reduced Stokes shift compared to **d7**. Locking the tertiary amine moiety in a planar conformation in the indoline system (compounds **d13-d14**) resulted in different effects depending on the system it was implemented. Compound **d13** showed reasonable red-shifted absorption characteristics and modest fluorescence. Increasing the strength of the acceptor group by using dicyanomethylene-pyranone, as in compound **d14**, resulted in a significant bathochromic shift in absorbance ($\lambda = 63$ nm in compound **d14** vs. compound **d13**) accompanied by the same large fluorescence shift but had very poor emission.

Interestingly, when compound **d7** was injected into a mouse and the dye bound to nerves were excited by either 405 nm or 447 nm laser, the wavelength dependent emission described above was observed (Figure 10). Excitation at longer wavelength (447 nm) showed a more pronounced red-shifted second peak. There were subtle differences between the in vivo (in mouse nerve) and in vitro (in DMSO solution) spectra of **d7**, which was expected because one medium is in solution while the other is in rigid tissue environment.

Conclusion

We have successfully screened a series of styryl- and distyryl dye systems (**d1-d14**) and identified three promising dyes (**d7**, **d9** and **d10**) that exhibit long wavelength emission, large Stokes shifts and reasonable fluorescence intensities while maintaining adequate solubility and high affinity to myelin. We observed an unusual wavelength-dependent dual emission behavior in which two distinct ground state conformers could individually be excited to favor emission from the locally excited (LE) or twisted intramolecular charge transfer (TICT) excited states in push-pull dye systems **d7**, **d9** and **d10**. Additionally, we observed an anomalous emission behavior of dye systems **d7** and **d8** under our study conditions, wherein the amino- derivative **d7** showed dual emission characteristic in polar medium, and the N,N-dimethyl derivative **d8** and the other N-alkylated derivatives **d12-d14**

did not show any TICT emission at all in either ground state or excited state. We envision that results presented here will elicit other research groups to elaborate on these photophysical observations.

The *in vivo* fluorescence imaging studies in rodents injected with selected dyes showed that visualization of nerves against a dark surrounding muscle tissue was possible. Because of their lipophilicity, the dyes also showed some non-specific uptake in adipose tissue, which appeared a different color than that of the nerves under multispectral imaging. These nerves were detectable while surrounded by fascia under fluorescence guidance.

Despite operating in the visible spectrum, we demonstrated that intraoperative fluorescence imaging in this optical window is a viable solution under certain conditions. For example, the large Stokes shift helps to minimize the impact of autofluorescence, similar to the approach taken in near-infrared imaging. Our future work on this class of dyes includes the development of derivatives that are less lipophilic, while maintaining their ability to cross the blood-nerve-barrier, in conjunction with applying novel strategies for differentiating the fluorescence of nerves from that of adipose tissue.

Supplementary Material

Refer to Web version on PubMed Central for supplementary material.

ACKNOWLEDGMENTS

We thank Bruce Johnson, Eric Williams, Jorge Ramos, Joseph Greene, Nicole LaPlante, Daniel Gray, and Kenneth Fish for technical assistance. This work is supported by NIH grant EB022872.

Biographies



Tiberiu Siclovan obtained his early education in chemical engineering from Timisoara Polytechnic, Romania. In 1992 he moved to the United States, and in 1996 received his Ph.D. in organic chemistry from Iowa State University under the direction of professor George A. Kraus. That same year he accepted a position at GE Global Research, where he is currently a senior scientist. His research interests include various aspects of biomedical and imaging technologies.



Rong Zhang received her B.S in chemistry from Nanjing University in China and her MS in organic chemistry from Worcester Polytechnic Institute. Prior to joining GE Global Research in 2005, she was a medicinal chemist at Abbott Laboratories. At GE Global Research, Rong is a lead chemist working on developing technologies and agents to enable diagnostic medical imaging.



Victoria Cotero received her B.S in chemistry from Fairleigh Dickinson University and her Ph.D. in pharmacology and human physiology from New Jersey Medical School, now Rutgers Medical School, in 2009. She then served as a postdoctoral fellow in neuroendocrinology/behavioral neuroscience at SUNY-Albany. At GE Global Research, Victoria is a lead biologist working on medical technologies for imaging and preclinical applications.



Anshika Bajaj obtained a B.S. in Pharmacy and M.S. in Biological sciences from BITS, Pilani, India in 2000, after which she moved to the United States to pursue a Ph.D. in Biochemistry from the University of Rochester. In 2006 she started her post-doctoral work at Albany Medical College and focused on studying signaling mechanisms involved in angiogenesis. She joined GE Global Research in 2010 where she contributed to and led biology tasks on multiple neuro, cell therapy, and immunotherapy projects. In 2015 she joined Immune Design a clinical stage immunotherapy company where she is responsible for in vitro characterization of lenti-



Dmitry V. Dyllov received his B.S. and M.S. degree in applied physics and mathematics from the Moscow Institute of Physics and Technology and Ph.D. from Princeton University in 2010. His research interests include theoretical aspects of imaging, spectroscopy and biophotonics.



Siavash Yazdanfar received his BS from Boston University and MS and PhD from Case Western Reserve University in biomedical engineering. Prior to joining GE in 2005, he was a postdoctoral fellow at the Massachusetts Institute of Technology. He has published 38 peer reviewed journal articles, 5 book chapters, and 22 issued US patents, primarily in the area of biomedical optical imaging and instrumentation.



Randall L. Carter received his B.S. in chemistry from the Pennsylvania State University and Ph.D. from Yale University in 1993. He served as an NIH post-doctoral fellow and visiting assistant professor at Duke University before joining GE Global Research in 1996. He is currently managing the Translational Sciences Laboratory with a research focus on the development of technologies and agents to enable diagnostic medical imaging.



Cristina Tan Hehir received her bachelor's degree in chemistry from the University of the Philippines Diliman. She obtained her Ph.D. in Chemistry/Biochemistry from Boston College and was a visiting associate at the Laboratory of Cell Biology at NHLBI/NIH. At GE Global Research, Tina is a senior scientist and project leader working on technologies for fluorescence guided surgery and development of imaging probes for neuroscience. She is also an NIH panel reviewer for Clinical Molecular Imaging Probe Development.



Arunkumar Natarajan obtained his B.S. degree in 1997 from Loyola College, Chennai, India and obtained his M.S. from the Indian Institute of Technology (IIT), Mumbai, India in 1999. Then he moved to the United States, and in 2005 obtained his Ph.D. from Tulane University. He continued his postdoctoral studies at UCLA from 2005-07. He joined GE Global Research in 2008, where he currently holds a lead scientist position. He has over 42 peer reviewed publications including 7 book chapters and 24-filed and 15-issued US patents. His scientific interests include photochemistry, polymers and materials chemistry for various technology applications including biological imaging, holography and additive manufacturing.

References

- [1]. Costello AJ, Brooks M, Cole OJ. Anatomical studies of the neurovascular bundle and cavernosal nerves. *BJU International*. 2004; 94(7):1071–1076. [PubMed: 15541130]
- [2]. Michaelson MD, Cotter SE, Gargollo PC, Zietman AL, Dahl DM, Smith MR. Management of Complications of Prostate Cancer Treatment. *CA: A Cancer Journal for Clinicians*. 2008; 58(4): 196–213. [PubMed: 18502900]
- [3]. Walz J, Graefen M, Huland H. Basic principles of anatomy for optimal surgical treatment of prostate cancer. *World Journal of Urology*. 2007; 25(1):31–38. [PubMed: 17333199]
- [4]. Aluffi P, Policarpo M, Cherovac C, Olina M, Dosdegani R, Pia F. Post-thyroidectomy superior laryngeal nerve injury. *European Archives of Oto-Rhino-Laryngology*. 2001; 258(9):451–454. [PubMed: 11769989]
- [5]. Cooper DS. Thyroxine Monotherapy After Thyroidectomy. *JAMA: The Journal of the American Medical Association*. Feb 20; 2008 299(7):817–819. 2008.
- [6]. Baker D, Conley J. Avoiding facial nerve injuries in rhytidectomy. Anatomical variations and pitfalls. *Plast Reconstr Surg*. 1979; 64(6):781–795. [PubMed: 515227]

- [7]. Warmuth M, Bowen G, Prosnitz L, et al. Complications of axillary lymph node dissection for carcinoma of the breast. *Cancer*. 1998; 83(7):1362–1368. [PubMed: 9762937]
- [8]. Thawait SK, Wang K, Subhawong TK, et al. Peripheral Nerve Surgery: The Role of High-Resolution MR Neurography. *American Journal of Neuroradiology*. Feb 1; 2012 33(2):203–210. 2012. [PubMed: 21527571]
- [9]. Kau T, Rabitsch E, Celedin S, et al. Feasibility and potential value of flat-panel detector-based computed tomography in myelography after spinal surgery. *Journal of Neurosurgery: Spine*. 2009; 10(1):66–72. [PubMed: 19119936]
- [10]. Bartels RHMA, Meulstee J, Verhagen WIM, Luttikhuis TTMC-O. Ultrasound imaging of the ulnar nerve: Correlation of preoperative and intraoperative dimensions. *Clinical Neurology and Neurosurgery*. 2008; 110(7):687–690. [PubMed: 18486322]
- [11]. Zhang T, Jiang W, Li Y, Li B, Yamakawa T. Perioperative Approach in the Surgical Management of Carotid Body Tumors. *Annals of Vascular Surgery*. 2012; 26(6):775–782. [PubMed: 22794331]
- [12]. Rais-Bahrami S, Levinson AW, Fried NM, et al. Optical Coherence Tomography of Cavernous Nerves: A Step Toward Real-Time Intraoperative Imaging During Nerve-Sparing Radical Prostatectomy. *Urology*. 2007; 72(1):198–204. [PubMed: 18280549]
- [13]. Schols R, Bouvy N, van Dam R, Stassen LS. Advanced intraoperative imaging methods for laparoscopic anatomy navigation: an overview. *Surg Endosc*. Jun 01; 2013 27(6):1851–1859. 2013. [PubMed: 23242493]
- [14]. Stankoff B, Wang Y, Bottlaender M, et al. Imaging of CNS myelin by positron-emission tomography. *Proc Natl Acad of Sci*. Jun 13; 2006 103(24):9304–9309. 2006. [PubMed: 16754874]
- [15]. Wu C, Tian D, Feng Y, et al. A Novel Fluorescent Probe That Is Brain Permeable and Selectively Binds to α -Myelin. *J. Histochem. Cytochem*. Sep 1; 2006 54(9):997–1004. 2006. [PubMed: 16709728]
- [16]. Wu C, Wei J, Tian D, Feng Y, Miller RH, Wang Y. Molecular Probes for Imaging Myelinated White Matter in CNS. *Journal of Medicinal Chemistry*. 2008; 51(21):6682–6688. [PubMed: 18844339]
- [17]. Bajaj A, LaPlante NE, Cotero VE, et al. Identification of the Protein Target of Myelin-Binding Ligands by Immunohistochemistry and Biochemical Analyses. *J Histochem Cytochem*. Jan 1; 2013 61(1):19–30. 2013. [PubMed: 23092790]
- [18]. Cotero V, Siclován T, Zhang R, et al. Intraoperative Fluorescence Imaging of Peripheral and Central Nerves Through a Myelin-Selective Contrast Agent. *Mol Imaging Biol*. 2012; 14(6):708–717. [PubMed: 22488576]
- [19]. Gibbs-Strauss S, Nasr K, Fish K, et al. Nerve-highlighting fluorescent contrast agents for image-guided surgery. *Mol Imaging*. 2011; 10(2):91–101. [PubMed: 21439254]
- [20]. Gray D, Kim J, Cotero V, et al. Dual-mode laparoscopic fluorescence image-guided surgery using a single camera. *Biomedical Optics Express*. 2012; 3(8):1880–1890. [PubMed: 22876351]
- [21]. Wang X, Bhaumik S, Li Q, Staudinger V, Yazdanfar S. Compact instrument for fluorescence image-guided surgery. *J. Biomed. Opt.* Apr 12.2010
- [22]. Gibbs SL, Xie Y, Goodwill HL, et al. Structure-Activity Relationship of Nerve-Highlighting Fluorophores. *PLOS One*. 2013; 8(9):e73493. [PubMed: 24039960]
- [23]. Chang Y, Chow T. Highly efficient red fluorescent dyes for organic light-emitting diodes. *J Mat Chem*. 2011; 21(9):3091–3099.
- [24]. Jana R, Pathak TP, Sigman MS. Advances in Transition Metal (Pd,Ni,Fe)-Catalyzed Cross-Coupling Reactions Using Alkyl-organometallics as Reaction Partners. *Chemical Reviews*. Mar 09; 2011 111(3):1417–1492. 2011. [PubMed: 21319862]
- [25]. Molnár Á . Efficient, Selective, and Recyclable Palladium Catalysts in Carbon–Carbon Coupling Reactions. *Chemical Reviews*. Mar 09; 2011 111(3):2251–2320. 2011. [PubMed: 21391571]
- [26]. Li, J. A Collection of Detailed Mechanisms and Synthetic Applications. Fourth Expanded. Springer-Verlag; Berlin Heidelberg; 2009. Name Reactions.

- [27]. Gray DC, Kim EM, Cotero VE, et al. Dual-mode laparoscopic fluorescence image-guided surgery using a single camera. *Biomed Opt Express*. 2012; 3(8):1880–1890. doi: 1810.1364/BOE.1883.001880. Epub 002012 Jul 001817. [PubMed: 22876351]
- [28]. Gray D, Kim E, Cotero V, Staudinger P, Yazdanfar S, Tan Hehir C. Compact fluorescence and white light imaging system for intraoperative visualization of nerves. *Proc SPIE*. 8207 Photonic Therapeutics and Diagnostics VIII2012.
- [29]. Ulf S, Heiner D. Synthesis and electronic spectra of substituted p-distyrylbenzenes for the use in light-emitting diodes. *Journal fuer Praktische Chemie*. 2000; 342(1):10–16.
- [30]. Saltiel J, Krishna T, Laohhasurayotin K, et al. Medium Effects on the Direct Cis-Trans Photoisomerization of 1,4-Diphenyl-1,3-butadiene in Solution. *Journal of Physical Chemistry A*. 2011; 115(11):2120–2129.
- [31]. Velsko S, Fleming G. *Chem Phys*. 1982; 76:3553–3562.
- [32]. Meier H, Gerold J, Kolshorn H, Muhling B. Extension of Conjugation Leading to Bathochromic or Hypsochromic Effects in OPV Series. *Chem. Eur. J*. 2004; 10:360–370. [PubMed: 14735504]
- [33]. Lapouyade R, Czeschka K, Majenz W, Rettig W, Gilabert E, Rullière C. Photophysics of donor-acceptor substituted stilbenes. A time-resolved fluorescence study using selectively bridged dimethylamino cyano model compounds. *Journal of Physical Chemistry*. 1992; 96:9643–9650.
- [34]. Letard J, Lapouyade R, Rettig W. *J. Am. Chem. Soc*. 1993; 115:2441–2447.
- [35]. Grabowski Z, Rotkiewicz K, Rettig W. Structural changes accompanying intramolecular electron transfer: focus on twisted intramolecular charge-transfer states and structures. *Chem. Rev*. 2003; 103:3899–4031. [PubMed: 14531716]
- [36]. Gruen H, Görner H. Fluorescence of Trans-Cyano-4'-dimethylaminostilbene; No Evidence for a TICT State. *Z Naturforsch*. 1983; 38 a:928–936.
- [37]. Pines D, Pines E, Rettig W. Dual fluorescence and excited state structural relaxations in donor-acceptor-stilbenes. *J. Phys. Chem. A*. 2003; 107:236–242.
- [38]. Atsbeha T, Mohammed A, Redi-Abshiro M. Excitation Wavelength Dependence of Dual Fluorescence of DMABN in Polar Solvents. *J Fluoresc*. Nov 01; 2010 20(6):1241–1248. 2010. [PubMed: 20473711]
- [39]. Catalan J. Can the dipolarity of the medium induce the formation of charge transfer structures? An unexpected finding in the photophysics of DMABN. *Physical Chemistry Chemical Physics*. 2014; 16(17):7734–7740. [PubMed: 24637990]
- [40]. Druzhinin SI, Demeter A, Galievsky VA, Yoshihara T, Zachariasse KA. Thermally Activated Internal Conversion with 4-(Dimethylamino)benzotrile, 4-(Methylamino)benzotrile, and 4-Aminobenzotrile in Alkane Solvents. No Correlation with Intramolecular Charge Transfer†. *The Journal of Physical Chemistry A*. Oct 01; 2003 107(40):8075–8085. 2003.
- [41]. Koch F, Heitz W. Soluble poly(1,4-phenylenevinylene)s and poly(1,4-phenyleneethynylene)s via Suzuki coupling. *Macromolecular Chemistry and Physics*. 1997; 198(5):1531–1544.
- [42]. Singh AK, Kanvah S. Photophysical studies of substituted 1,2-diarylethenes: twisted intramolecular charge transfer fluorescence in dimethoxycyano-substituted 1,2-diarylethene. *Journal of the Chemical Society, Perkin Transactions 2*. 2001; (3):395–401.
- [43]. Fromherz P, Heilemann A. Twisted internal charge transfer in (aminophenyl)pyridinium. *The Journal of Physical Chemistry*. Aug 01; 1992 96(17):6864–6866. 1992.
- [44]. Nag A, Kundu T, Bhattacharyya K. Effect of solvent polarity on the yield of twisted intramolecular charge transfer (TICT) emission. Competition between formation and nonradiative decay of the TICT state. *Chemical Physics Letters*. 1989; 160(3):257–260.
- [45]. Strehmel B, Seifert H, Rettig W. Photophysical Properties of Fluorescence Probes. 2. A Model of Multiple Fluorescence for Stilbazolium Dyes Studied by Global Analysis and Quantum Chemical Calculations†. *The Journal of Physical Chemistry B*. Mar 01; 1997 101(12):2232–2243. 1997.

Highlights

Synthesized and investigated photophysical properties of several substituted styryl type dyes **d1-d15**.

Three dyes **d7**, **d9** and **d10** showed good fluorescent properties and maintained drug-like binding property.

Observed an unusual dual emission behavior with two distinct ground state conformers that could individually be excited.

Observed an anomalous emission behavior on dye systems **d7** and **d8** the amino-derivative **d7** showed a dual emission characteristic in the polar medium, while the N,N-dimethyl derivative **d8** did not.

Interestingly, when compound **d7** was injected into a mouse and the dye bound to nerves were excited by either 405 nm or 447 nm laser, a wavelength dependent emission described above was observed similar to fluorescence in DMSO.

in-vivo fluorescence imaging studies in rodents using small animal multispectral imaging instrument and the dual-mode laparoscopic instrument developed in-house.

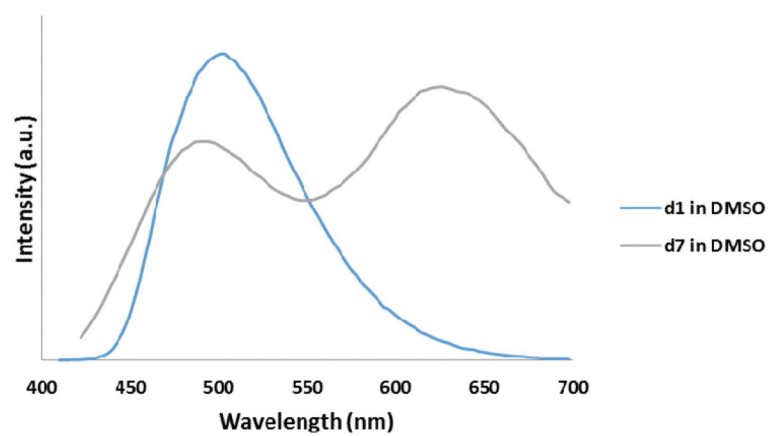


Figure 1.
Overlay of emission of *d1* and *d7* in Toluene (A) and in DMSO (B)

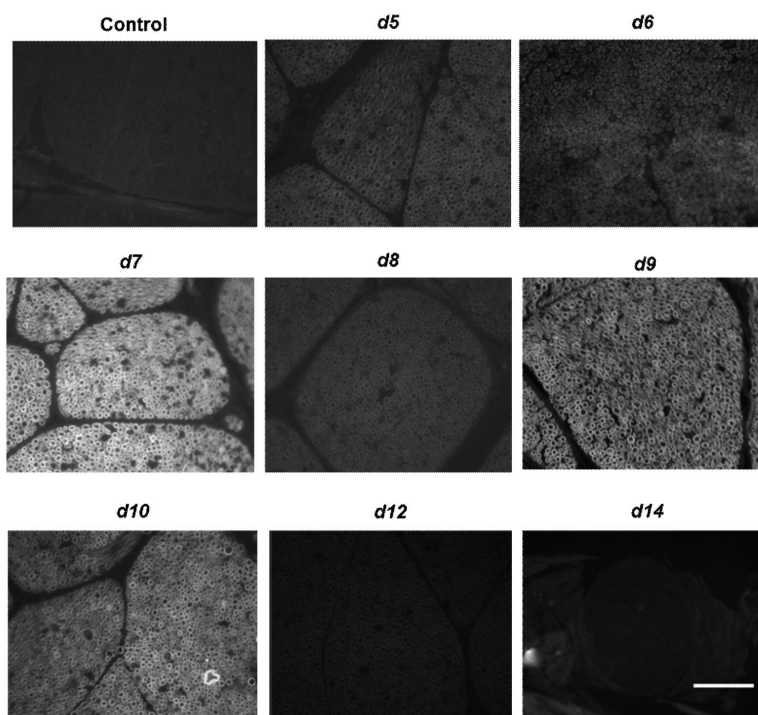


Figure 2. Qualitative ex vivo nerve labeling screening of several fluorophores. 10 μ M of each dye was incubated with rat nerve tissue sections to assess their ability to stain the myelin bundles by fluorescence microscopy. The control tissue was incubated with buffer only. Scale bar \sim 50 μ m.

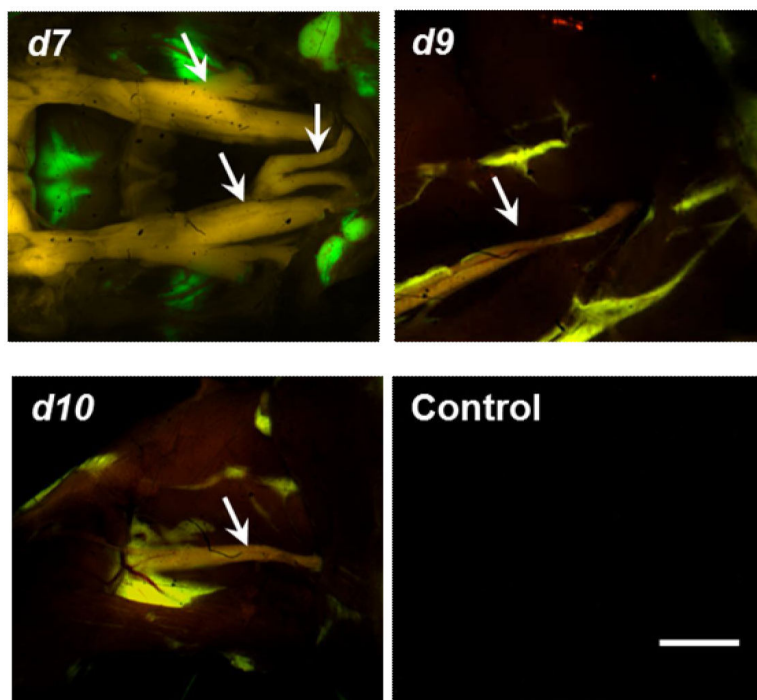


Figure 3.

In vivo multispectral imaging of mice injected with *d7* (GE3082), *d9* (GE3111), or *d10* (GE3126). The control animal received injection buffer only, and imaged under the same conditions as the dye-treated mice. Arrows are pointing to the trigeminal and optic nerves (*d7*) and to the sciatic nerve (*d9*, *d10*). Scale bar ~ 1 mm.

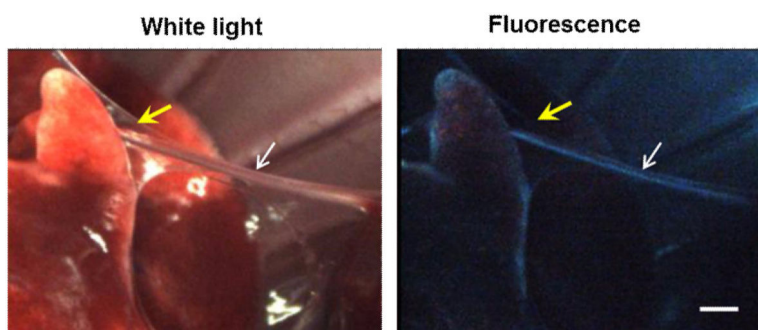


Figure 4. Simultaneous dual-mode (white light and fluorescence laparoscopic imaging of the thoracic cavity of a rat injected with *d7* (GE3082). The white arrows are pointing to the phrenic nerve, and yellow arrows are pointing to a layer of fascia surrounding the nerve. Scale bar ~1 mm.

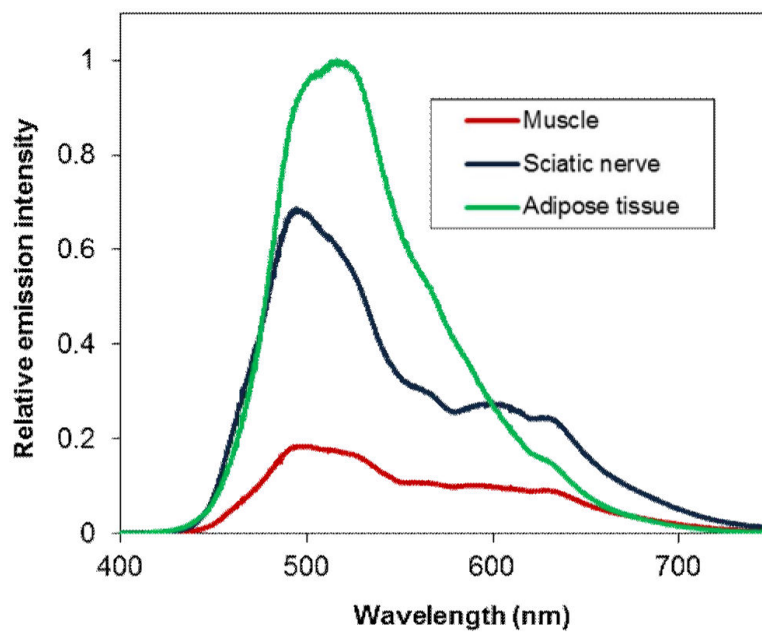


Figure 5. Fluorescence emission spectra of nerve, adipose tissue, and muscle of a mouse injected with *d10* (GE3126).

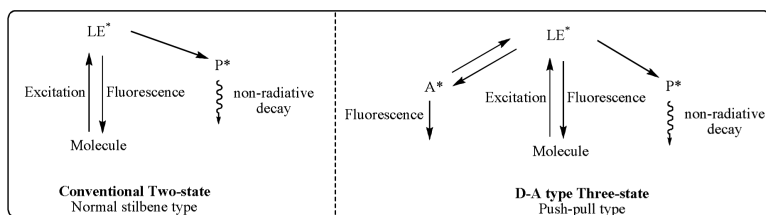


Figure 6. Interpretation of photophysical behavior of push-pull stilbenes (Left) Conventional Two-State and (Right) Proposed Three-State Kinetic Scheme.

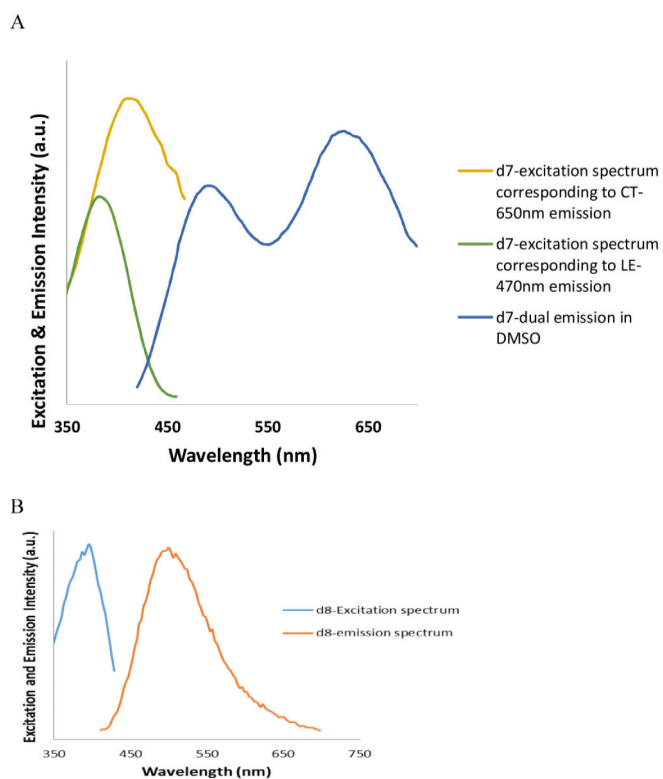


Figure 7. Excitation and emission spectra of compounds *d7* (A) and *d8* (B). *d7* shows two distinct excitation peaks corresponding to LE and TICT state emission in DMSO, while and compound *d8* shows only one excitation and emission corresponding to the LE state.

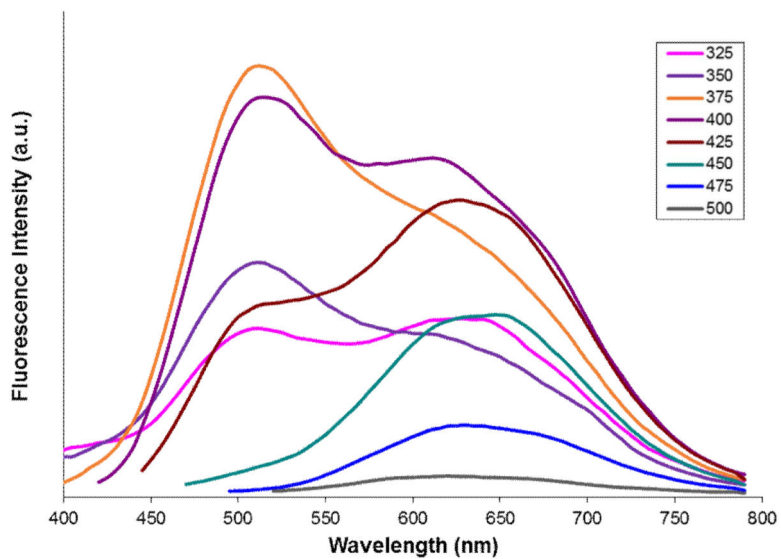


Figure 8. Wavelength dependent dual-emission spectrum of compound *d7* (GE3082) showing the presence of two distinct conformers in the ground state with different population levels.

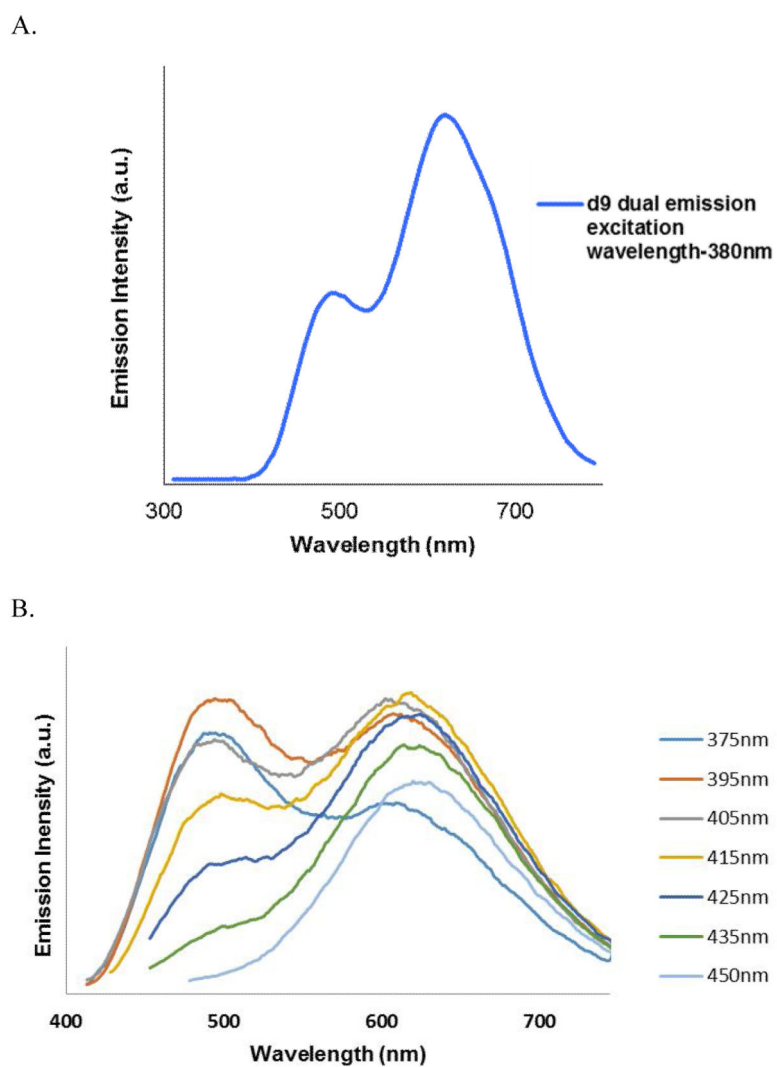


Figure 9.

A. Dual-emission seen in compound *d9*. Emission obtained using excitation wavelength-380 nm. **B.** Wavelength dependent dual-emission spectrum of compound *d10* showing presence of two distinct conformers in the ground state with different population.

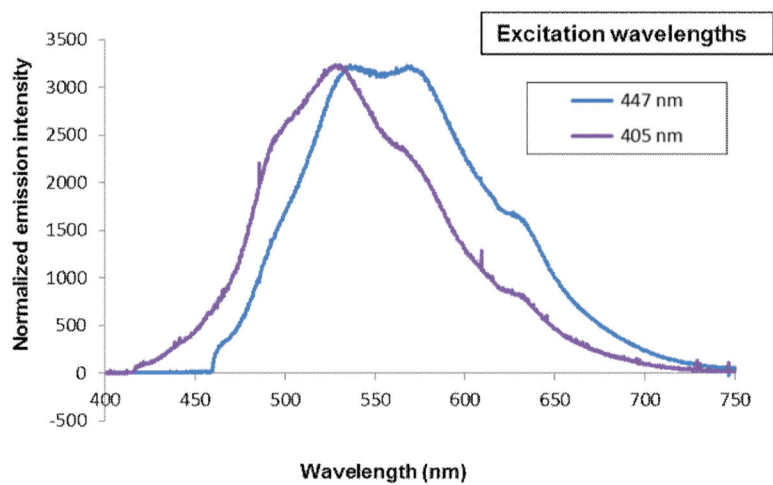
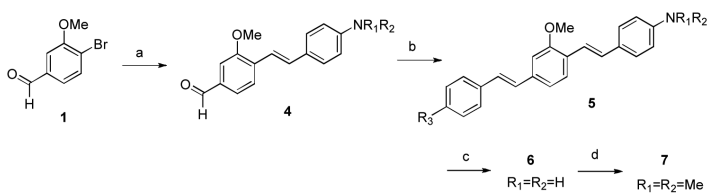
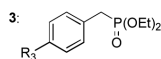
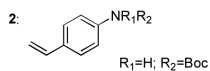


Figure 10. Wavelength dependent emission spectrum of compound *d7* (GE3082) in the sciatic nerve of a mouse injected with *d7*.



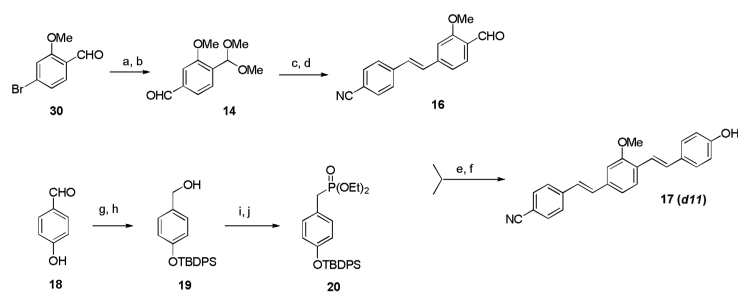
a: **2**, Pd(OAc)₂, TPPTS, K₂CO₃, DMF/H₂O, 95°C, 3hrs, 70%; **b**: **3**, tBuOK, THF; **c**: TFA/CH₂Cl₂-amylene or 4N HCl, dioxane; **d**: CH₂O, NaBH(OAc)₃, CH₂ClCH₂Cl



TPPTS: tris-(3-sulphonatophenyl)phosphine

Scheme 1.

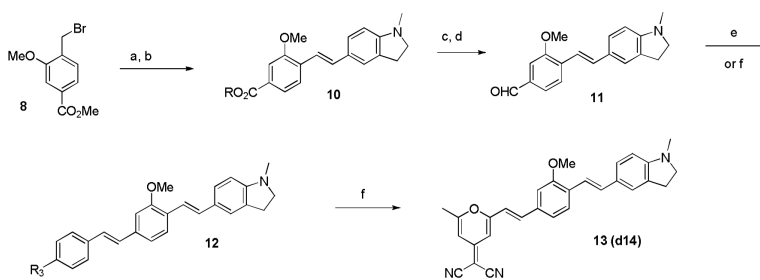
Synthesis of D-A bis-styryl dyes **d7-d10** and their analogs **d7**: R₁=R₂=H, R₃=CN; **d8**: R₁=R₂=Me, R₃=CN; **d9**: R₁=R₂=H, R₃=MeSO₂; **d10**: R₁=R₂=H, R₃=N'-(2-hydroxyethyl)-N-piperazinylsulfonyl.



a: $\text{HC}(\text{OMe})_3$, MeOH, cat. PTSA, reflux, 3h, 96%; b: nBuLi, N-formylpiperidine, Et_2O , -30°C to -78°C , 1h, 92%; c: **15**, tBuOK, THF, 60°C , 1h, 80%; d: cat. PTSA, THF/ H_2O 80/20, 60°C , 1h, 95%; e: **20**, tBuOK, THF, 60°C , 1h; f: 2 eq. AcOH, SiO_2 , chromatography, 68%; g: TBDPSCl, imidazole, $\text{CH}_2\text{Cl}_2/\text{DMF}$ 10/1, o/n, 71%; h: NaBH_4 , MeOH, 0°C , 2h, 95%; i: 0.5 eq. PBr_3 , CH_2Cl_2 , 0°C , 3h; j: $\text{P}(\text{OEt})_3$, 100°C , 2h, 62% over two steps.

PTSA: p-Toluenesulfonic acid; TBDPSCl: tert-Butyldiphenylsilyl chloride; **15**: diethyl-4-cyanobenzyl phosphonate

Scheme 2. Synthesis of compound *d11*

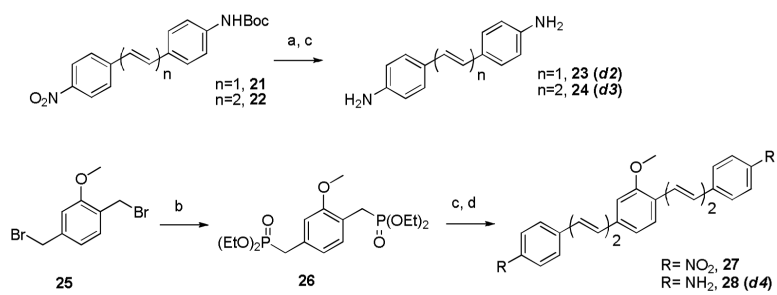


a: $P(OEt)_3$, $100^\circ C$, 2 hrs, 98%; b: **9**, tBuOK, THF, 94%; c: $LiAlH_4$, THF, 68%; d: NMO, TPAP, CH_2Cl_2 , MS3A, 62%; e: aryl phosphonate, tBuOK, THF; f: active methylene compound, 0.05 eq, piperidine, EtOH $80^\circ C$.

9: N-methyl-5-formylindoline; NMO: N-methylmorpholine-N-oxide; TPAP: tetra*N*-propylammonium perruthenate; MS: molecular sieves

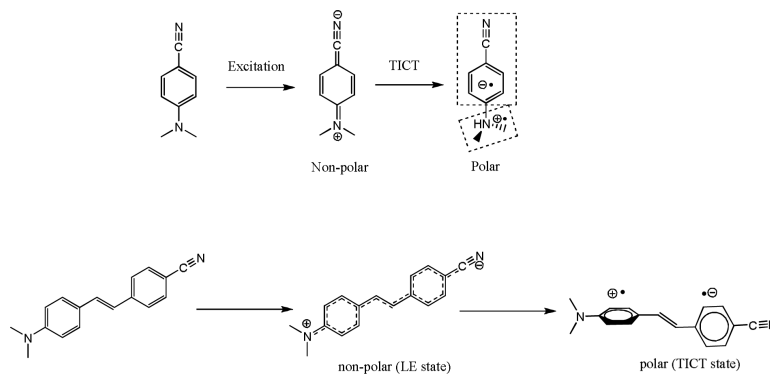
Scheme 3.

Synthesis of dyes bearing multiple electron-withdrawing groups

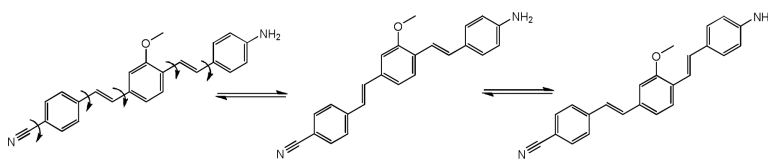


a: 4N HCl-dioxane, 0°C-r.t., 72-74%; b: P(OEt)₃, 100°C, 1h, 90%; c: *trans*-4-nitrocinnamaldehyde, t-BuOK, diglyme, 100°C, 3h, 73%; d: Zn, NH₄Cl, DMF, 85°C, 12h, 58%.

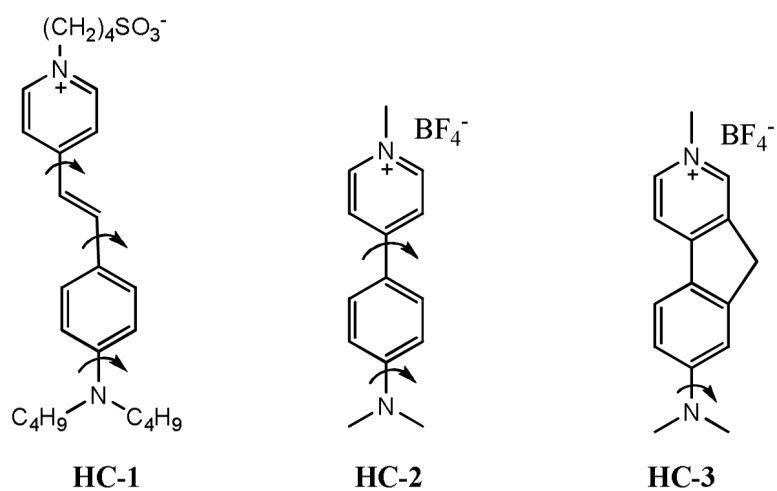
Scheme 4.
 Synthesis of styryl and polyene dyes **d2-d4**

**Scheme 5.**

Access of TICT state in polar medium *via* Intramolecular N,N-dimethyl- group twisting of DMABN in polar medium and anilino- group twisting in push-pull stilbenes.



Scheme 6.
Possibility of multiple ground state conformations (rotamers) due to single bond rotations in push-pull tri ring systems.

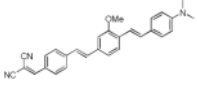
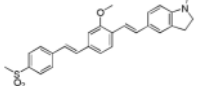
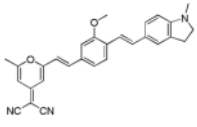
**Scheme 7.**

Dependence of bond rotations on TICT emission resulting in non-Fluorescent TICT (**HC-1**); weakly fluorescent (**HC-2**) and strongly fluorescent (**HC-3**).

Table 1

Styryl and bis-styryl fluorophores in solution

Name ^a	Chemical Structure	λ_{Abs} , nm ^b	λ_{Em} , nm ^c (Intensity) ^d
<i>d1</i> (BMB) ^a		408	495 (106,800)
<i>d2</i>		362	414 (246,900)
<i>d3</i>		383	448 (84,300)
<i>d4</i>		400	575 (200)
<i>d5</i>		415	511 (93,300)
<i>d6</i>		385	522 (2,800)
<i>d7</i> (GE3082) ^a		417	491, 621* (1,700; 2,520*)
<i>d8</i>		412	518 (264)
<i>d9</i> (GE3111) ^a		412	480, 624* (2,250; 4,700*)
<i>d10</i> (GE3126) ^a		414	510, 618* (2,100; 3,970*)
<i>d11</i>		396	532 (12,640)

Name ^a	Chemical Structure	λ_{Abs} , nm ^b	λ_{Em} , nm (Intensity) ^d
d12		467	582 (180)
d13		419	533 (2,900)
d14		482	649 (150)

^aThe d-numbering scheme for each dye is used for simplicity. For previously published fluorophores, the original designations are shown in parenthesis.

^bAbsorbance maximum wavelength measured in DMSO

^cEmission maximum wavelength measured in DMSO, the relative fluorescence intensity at the maximum wavelength shown in parenthesis

^dRelative emission intensity values at λ_{Em} RFU. For dual emissions, the emission intensities in parentheses correspond to the λ_{Em} shown, respectively.

* Dual emission (TICT) in polar solvents.